POLITECNICO DI TORINO
Repository ISTITUZIONALE

A Methodology for the Dimensional and Mechanical Analysis of Surgical Guides

Original
A Methodology for the Dimensional and Mechanical Analysis of Surgical Guides / Salerno, F., Moos, S., Ulrich, L., Novaresio, A., Vezzetti, E.. - (2024), pp. 184-193. (3rd International Conference on Design Tools and Methods in Industrial Engineering, ADM 2023) [10.1007/978-3-031-52075-4_22].

Availability:
This version is available at: 11583/2987386 since: 2024-12-07T14:09:14Z

Publisher:
Springer

Published
DOI:10.1007/978-3-031-52075-4_22

Terms of use:

This article is made available under terms and conditions as specified in the corresponding bibliographic description in the repository

Publisher copyright
Springer postprint/Author's Accepted Manuscript

This version of the article has been accepted for publication, after peer review (when applicable) and is subject to Springer Nature's AM terms of use, but is not the Version of Record and does not reflect post-acceptance improvements, or any corrections. The Version of Record is available online at: http://dx.doi.org/10.1007/978-3-031-52075-4_22

(Article begins on next page)

24 October 2026

A Methodology for the Dimensional and Mechanical Analysis of Surgical Guides

Federico Salerno[1*][0000−0001−5282−9513], Sandro Moos[1][0000−0001−5097−7344], Luca Ulrich[1][0000−0001−8407−0660], Andrea Novaresio[1], and Enrico Vezzetti[1][0000−0001−8910−7020]

[1]Politecnico di Torino, Department of Management and Production Engineering, C.so Duca degli Abruzzi, 24, Torino, 10129, Italy
[*]Corresponding author email: federico.salerno@polito.it;
Contributing author emails: sandro.moos@polito.it; luca.ulrich@polito.it; andrea.novaresio@polito.it; enrico.vezzetti@polito.it.

Abstract. The use of CAD and 3D printing of surgical guides (SGs) for osteotomies is a widely developed practice in orthopaedic surgery, and particularly in maxillo-facial interventions, but validation studies rarely occur in literature. The present study defines a methodology to validate SGs dimensionally and mechanically through geometrical analysis, tensile testing, contact simulations, and abrasion testing. Distortions between the 3D printed SGs and the CAD model are quantified and an average deviation error for each production process step is obtained. Mechanical analysis identifies a way of applying the load on the SG to measure their equivalent linear stiffness (N/mm), maximum displacement (mm) and corresponding tolerable load (N) by varying some dimensional parameters. The stress state was assessed by finite element method (FEM) analysis, then the numerical results were compared with experimental ones using tensile tests: stiffness, maximum displacement and the corresponding loads were evaluated. The distribution of contact pressure on soft tissues was obtained numerically by FEM analysis. Finally, an ad hoc machine has been specially built to engrave discoidal specimens with typical operating room conditions. The methodology has been validated using 11 SG fibular and mandibular specimens and reporting the obtained results of each procedure step.

Keywords: Surgical guides · Cutting guides · Maxillo-facial surgery · CAD · FEM.

1 Introduction

Orthopedic surgery often requires performing precise cuts in bone tissue, such as the removal of bone tissue tumors [1], bone flaps distraction [2], and repositioning [3]. In maxillo-facial surgery, the accuracy and precision of osteotomies are critical for proper execution of the surgery [4], as well as for the patient's aesthetics [5].

Within Virtual surgical planning (VSP) a 3D anatomical model is built from the CT data using appropriate medical segmentation software. Surgical guides (SGs) are patient-specific tools that are fixed to patient's bone through special screws and are used to guide the cutting tool performing the osteotomies [6,7]. To guarantee a proper outcome the SGs must satisfy many requirements such as the dimensional discrepancies between the CAD model and the 3D printed SGs must be limited, the material must bear external forces, tightening torque [8,9] and abrasive cutting action [10]. Also SGs should evenly apply a pressure distribution over the underlying tissues to avoid damage.

This paper aims to address the design challenges by presenting an integrated methodology to validate SGs accordingly to various aspects of EU regulations. EU Regulation 2017/745, Annex I, Chapter II "Requirements regarding design and manufacture" requires tolerance and tensile analyses, EU Regulation 2017/745 Article 61 and Annex XIV requires contact pressure simulations, and EU Regulation 2017/745, Annex I, Chapter II requires abrasion testing.

SG geometrical analysis are not a novelty in the literature [11,12], especially regarding bio-compatible materials and their properties [13]. In this work the dimensional control is aimed to evaluate how tolerances evolve through the various production stages performing tests carried out numerically and experimentally.

The abrasion resistance of the SGs must be evaluated, because a piezoelectric vibrating blade is used to perform osteotomies [14]. In the literature there are several articles about abrasion tests (ASTM G65) on polymeric materials [15], but the methodology here presented evaluates the abrasion resistance of the SGs in the operating room working conditions.

2 Materials and methods

Geometry: the effects of the various processes over the real geometry are estimated through a dimensional analysis, identifying the following four temporal instants: T1, CAD models of SGs; T2, SGs after 3D printing; T3, SGs after full polymerization by UV rays; T4, SGs after sterilization. T3 can be skipped for polymers that are not photosensitive.

Geometric tolerances and *datum* reference frames (DRFs) are identified on the CAD model accordingly to Fig. 1. The 3D printed part is scanned and the triangulated point cloud is aligned with the CAD model to assess deviations. T2, T3 and T4 triangulated point clouds are compared to the T1 CAD model in order to evaluate how the geometry evolves during production steps. The distance of all the points of the surface to be checked from the counterpart of the CAD model was evaluated to measure the profile tolerances. For each SG, the tolerances T_i in Fig. 1 are measured at T2, T3, and T4. Calling n the total number of T_i for each SG, the average tolerance AT for each instant is calculated as follows:

$$\mathrm{AT} = \frac{\sum_{i=1}^{n} \mathrm{T}_i}{n} \tag{1}$$

For the sake of clarity, an overall average tolerance (OAT) value is calculated by considering the T2, T3, and T4 time points, in order to obtain a comprehensive measure of the tolerance caused by each production step. Calling m the total number of SG, OAT value is calculated as follows:

$$\mathrm{OAT} = \frac{\sum_{j=1}^{m} \mathrm{AT}_j}{m} \tag{2}$$

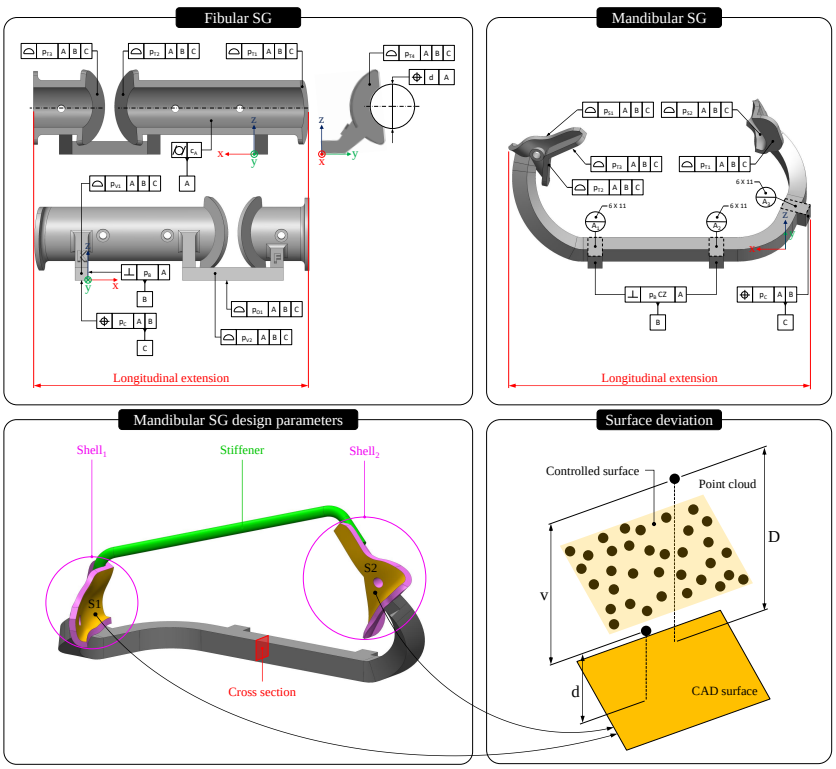

Fig. 1. DRFs, geometric tolerances T_i to be inspected and surface deviations. Fibular SG on the top-left and mandibular SG on the top-right. On the bottom-left, design parameters of mandibular SG are shown and on the bottom right, a scheme of surface deviations dev_{S1} and dev_{S2} is provided, where D is the maximum signed distance, d is the minimum signed one, while v is the maximum variation of distance between points of scanned surface and CAD counterpart

Furthermore, deviations in shell-bone adhesion surface, denoted as dev_{S1} and dev_{S2}, are compared among three different design variants applied to mandibular SGs: 1) without an additional stiffener connecting the two shells, 2) with a stiffener, and 3) with the stiffener removed after T4. Additionally, the first variant includes three different cross-section values, namely $6 \times 6\,\mathrm{mm}$, $7 \times 7\,\mathrm{mm}$,

and 8×8 mm. To measure the deviations, the distance of all the points of the surface to be checked from the counterpart of the CAD model are evaluated. Calling D the maximum distance, d the minimum one, and m the mean of the distances, surface deviations are calculated as follows (Fig. 1 right):

$$dev_{S1}, dev_{S2} = m \pm \frac{v}{2}, \text{ where: } v = \begin{cases} D & \text{if } D, d \geq 0 \\ D - d & \text{if } D \geq 0 \text{and } d \leq 0 \\ d & \text{if } D, d \leq 0 \end{cases} \quad (3)$$

Stress field: given the complex geometry of the SGs it is necessary a FEM simulation to calculate the material tensile field when subjected to external forces under operative conditions. A virtual tensile test is simulated and the results are compared to a real physical test for the validation. The FEM simulation precisely reproduces the tensile test setup: each end of the SG is connected to the respective clamp of the traction machine through a chain of 4 elements. The first is a 3D printed PLA interface element that replicates the SG support surface, the second is a connecting bolt to rigidly connect the SGs with the interface, the third is a steel plate that connects the clamp to the interface, while the fourth is a steel pin thanks to which the interface is hinged to the plate. Specifically, the bolts are modeled as "beam elements" and an axial preload of 300 N is applied to simulate the bolt effect. The steel plate is clenched in the vise of the testing machine. The layout, the traction axis and the mechanical constraints are identified as in Fig. 2.

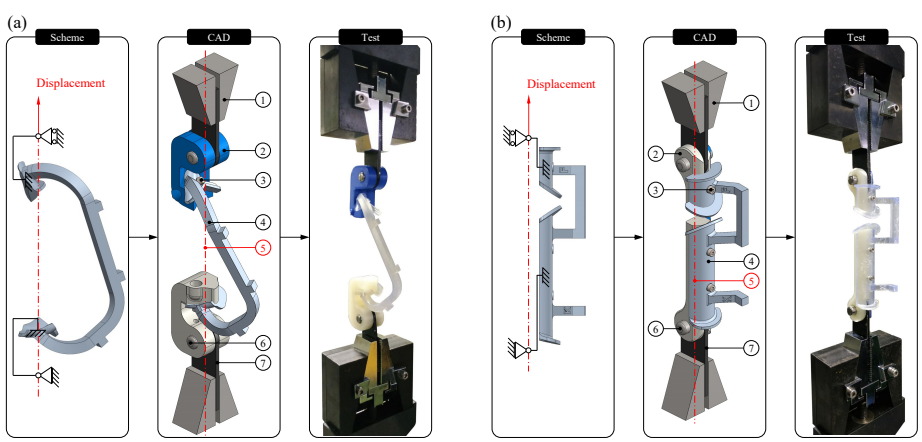

Fig. 2. Mechanical resistance test for mandibular (a) and fibular (b) SGs. (1) clamps, (2)interface, (3) threaded connection, (4) SG, (5) traction virtual axis, (6) steel pin and (7) steel plate.

The deformation rate of the virtual simulation is equal to that one of the real test. Von Mises stress field and force reactions at vise constraints are evaluated. Finally, the engineering stress-strain curves of the virtual and physical simulation are compared to validate the FEM model.

Contact pressure on soft tissue: For safety reasons, clinicians typically strive to preserve a thin layer of soft tissue surrounding the bone, where the SGs will be attached. This practice helps prevent bone tissue necrosis. The geometry is characterized as a set of three overlapped layers where the topmost is the surgical guide shell, the underlying layer is soft tissue and the lowest layer is bone tissue, with the geometry that conforms to the patient anatomy.

Soft tissue is characterized as a linear isotropic elastic material, according to Aloy at al. (2017) [16], with Young's modulus equal to 12 MPa, while bone is defined as linear isotropic elastic material with a Young modulus of 2.1 GPa and a breaking load of 14 MPa, according to Zerdzicki et al (2021) [17]. Contact constraints between layers are inserted: bonded contacts are used to simulate the interaction between the bone and soft tissues. The contact interaction between SGs and soft tissue allows reciprocal sliding and distancing, setting 0.1 as friction coefficient. To simulate continuity with the surrounding material while reducing computational complexity, a superficial stiffness distribution (Ansys elastic foundation stiffness (EFS)) is set around both the soft and bone tissue with the following parameters: $\mathrm{EFS}_{\text{Soft tissue}} = 0.04\,\mathrm{N/mm^3}$ and $\mathrm{EFS}_{\text{Bone tissue}} = 7.71\,\mathrm{N/mm^3}$. Finally a preload of 50 N is applied to each threaded connection. The pressure map in the contact regions between SGs and soft tissue is then calculated.

Abrasion: the proposed method involves the construction of a *ad hoc* machine (Fig. 3). The machine consists of a wooden base with two vertical steel cylindrical guides, a slider mounted on these guides, and a stepper motor NEMA 17 42-34 affixed to the base, capable of Y-axis movement via a rail. The motor shaft accommodates Discoidal Clear V1 biomed samples. Custom components were developed with Solidworks CAD and 3D printed on a Prusa i3 MK3s using PLA. To lower sliding friction, linear bearings are utilized. An Aesculap GBL30R surgical piezoelectric handpiece, equipped with a blade, is attached to the slider. A vertical metal plate, connected to the guides by a crossbar, enhances the structure's stiffness. The handpiece and blade, along with the slider and bearings, form a movable assembly. A dynamometer and an adjustable mass counterweight are connected to this assembly via two rotating pulleys and a wire. The load on the sample, labeled as P, can be increased by reducing the mass of the counterweight. When the counterweight mass balances the moving assembly, $P = 0\,\mathrm{g}$. The dynamometer allows direct reading of the counterweight value. Positioned at a 15° angle to the Z axis, the handpiece and blade favor material abrasion while mitigating the stick-slip effect.

The test procedure involves the following steps: 1) specimen initial mass measurement, m_i; 2) P calibration by adjusting the counterweight mass; 3) motor activation at constant rotation speed $n = 30\,\mathrm{rpm}$ and simultaneous handpiece activation to make the blade vibrate; 4) handpiece and motor are stopped after a

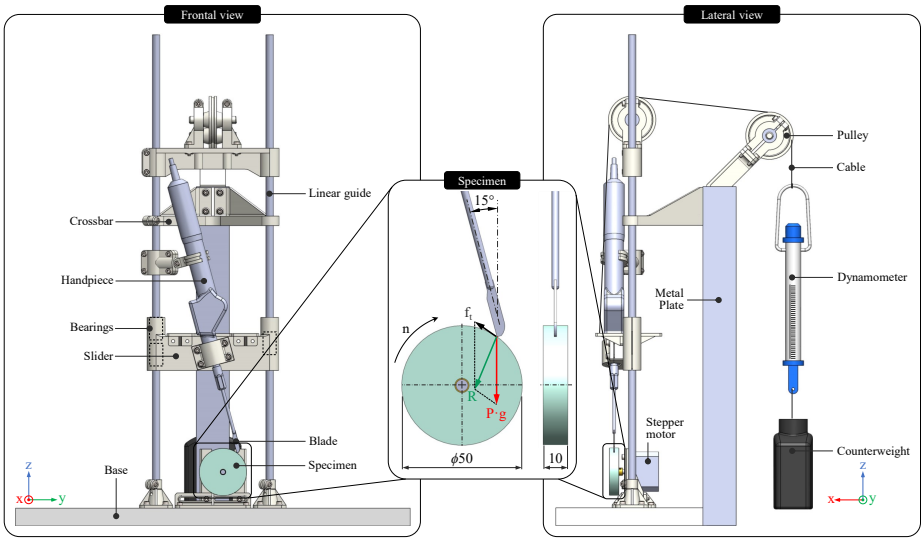

Fig. 3. Abrasion testing machine : a frontal view (left) and a later one (right); the central detail shows the blade tilt, forces between blade and specimen and the dimensions of the latter.

predefined number of revolutions; 5) specimen is removed and its final mass m_f is measured. The tests were repeated four times, increasing P, on two specimens each, measuring the mass reduction. The abrasion coefficient a is defined by Eq. 4, while the material removal rate (MRR) by Eq. 5, where t is the abrasion time ($t = 12\,\mathrm{s}$):

$$a = \frac{m_i - m_f}{m_i} \cdot 100 \qquad (4) \qquad\qquad \mathrm{MRR} = \frac{m_i - m_f}{t} \qquad (5)$$

3 Results and discussion

A review of literature and commercial sources lead to six materials, biocompatible, compliant to the EN ISO Standards 10993 and 18562 for class IIa applications. The one selected for the present tests is Formlabs BioMed Clear printed using Formlabs 3B+ SLA printer.

The dimensional analysis comprised 11 SG specimens, 5 fibular and 6 mandibular. The sterilization process lasted 20 min at 134 ºC and 30 min at 121 ºC.

In the left graph of Fig. 4, bars represent AT values, while the longitudinal extensions are represented by blue markers for both fibular and mandibular SGs. OAT in T2, T3 and T4 is 0.70 mm, 0.67 mm and 0.96 mm, respectively. By performing a one-tailed Student's t-test and assuming a significance level of 0.05, p-values are calculated. There is a significant difference between T3 and T4 ($p = 0.0007$), but not between T2 and T3 ($p = 0.3041$). Furthermore, for both

fibular and surgical SG, there is a significant correlation between longitudinal extension and average tolerance in T4 ($p = 0.0023$ for fibular and $p < 0.0001$ for surgical SG). Deviations dev_{S2} of mandibular SG has a peak with 7×7 mm cross section: $m = 3.89$ mm and $v = 14.16$ mm. Conversely, by inserting and removing the bridge dev_{S2} is equal to 0.27 mm and 3.32 mm for m and v, respectively (Fig. 4 right). Results show that removing the support bridge after sterilization is preferable to increase the cross-sectional area of the handle section and, consequently, enhance the dimensional stability.

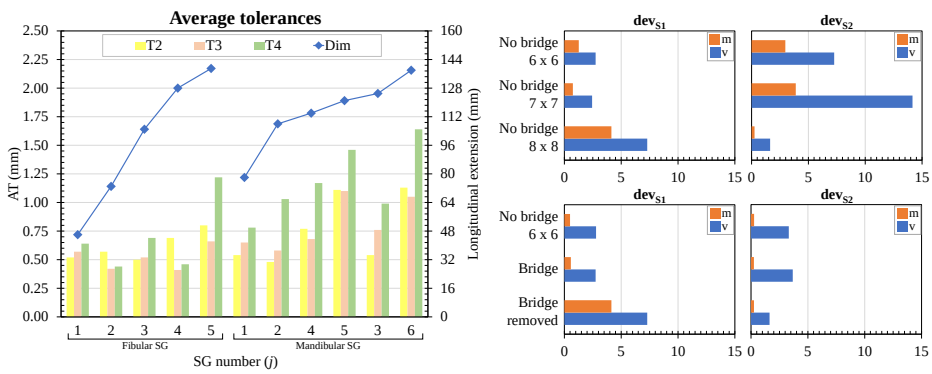

Fig. 4. Left: average tolerances AV and longitudinal extension (mm) for fibular and mandibular SGs at T2, T3 and T4 instants; Right: m and v values of surface deviations dev_{S1} and dev_{S2} by varying design parameters.

The mechanical evaluation was performed on mandibular SG variants with a cross sections of 6×6 mm, 7×7 mm, 8×8 mm and one fibular SG.

As for the simulations, a FEM analysis using the software ANSYS Workbench was performed. A total of 16 specimens were tested: 5 for SG 6×6 mm, 3 for SG 7×7 mm, 3 for SG 8×8 mm and 5 for fibular SG. The tensile test, force-displacement curves for both experimental and numerical tests are shown in Fig. 5.

As we could expect a proportional correlation within mean experimental stiffness values and cross section size was found. The curves match appropriately before the ultimate tensile strength (UTS) declared by the supplier (52 MPa), so it is possible to validate FEM analysis under that load limit. Moreover, graphs of Fig. 5 show that the material is able to sustain higher loads. With respect to contact pressure field on soft tissues, mandibular SG has a peak pressure of 0.47 MPa which falls between the two holes (Fig. 6 top-left). On the other hand, in the fibular SG, the maximum pressure amounts to 0.156 MPa (Fig. 6 bottom-left). These results can be considered safe for the patient according to the literature [18]. Fig. 6 show $a-P$ and MRR$-P$ correlations: a varies between

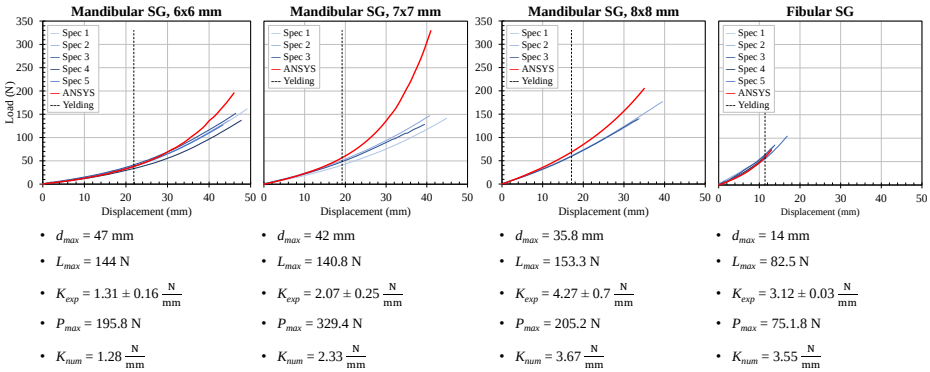

Fig. 5. Experimental (blue) and numerical (red) force-displacement curves obtained from both tensile test and ANSYS Workbench simulations. d_{max}: elongation at break L_{max}: numerical load corresponding to the elongation at fracture K_{exp}: experimental linear stiffness P_{max}: experimental load corresponding to the elongation at fracture K_{num}: numerical linear stiffness .

0.023 % and 0.033 % by adjusting P from 225 g to 325 g. The corresponding MRR for the latter load values are 0.032 g/min and 0.045 g/min, respectively.

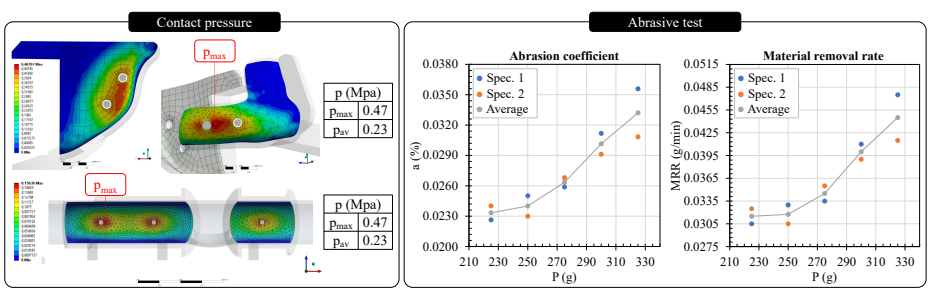

Fig. 6. Contact pressure and abrasion test results. (left): pressure distribution on contact surface caused by SG fixation on the patient, on the top mandibular SG and on the bottom fibular SG; (right): $a - P$ and MRR $- P$ correlations, where a is the abrasion coefficient, MRR is the removal material rate and P is the load on the sample.

4 Conclusions and future works

In conclusion, we proposed a methodology for the quality control of CAD-modeled and SLA 3D-printed surgical guides for maxillo-facial surgery. Through

tolerance analysis, tensile testing, contact simulations, and abrasion testing, we evaluated both the geometric and mechanical properties of SGs. Our study found that sterilization was the main source of dimensional distortion and that changing design parameters could improve both the dimensional stability and the stiffness of SGs. Furthermore, we found that the maximum pressure on mandibular and fibular SGs during tensile testing was safe for patients. Finally, our abrasion testing methodology aimed to predict the abrasion resistance of SGs using the same instrument as in the operating room. Although our work has some limitations, it provides a valuable contribution to the quality control of SGs and highlights the need for further research in characterizing the plastic behavior of surgical guide polymers. The future work should be focused on addressing the following limitations: more specimens for each type of SG should be tested in order to carry out statistical evaluations; further resources should be allocated to characterize the resin through a campaign of tensile tests on unified samples; our study assumed that soft and bone tissues were isotropic and elastic materials without considering nonlinear behavior.

References

1. Martin Schulze, Georg Gosheger, Sebastian Bockholt, Marieke De Vaal, Tymo Budny, Max Tönnemann, Jan Pützler, Albert Schulze Bövingloh, Robert Rischen, Vincent Hofbauer, Timo Lübben, Niklas Deventer, and Helmut Ahrens. Complex Bone Tumors of the Trunk—The Role of 3D Printing and Navigation in Tumor Orthopedics: A Case Series and Review of the Literature. *Journal of Personalized Medicine*, 11(6):517, June 2021.
2. Aydin Gülses, Metin Sencimen, Mustafa Ayna, Matthias Gierloff, and Yahya Açil. Distraction histogenesis of the maxillofacial region. *Oral and Maxillofacial Surgery*, 19(3):221–228, September 2015.
3. Corine J. Samaha, Hiba J. Tannous, Diane Salman, Joseph G. Ghafari, and Jason Amatoury. Role of surgical hyoid bone repositioning in modifying upper airway collapsibility. *Frontiers in Physiology*, 13, 2022.
4. Kunihiro Oka, Tsuyoshi Murase, Hisao Moritomo, Akira Goto, Ryoji Nakao, Hideki Yoshikawa, and Kazuomi Sugamoto. Accuracy of corrective osteotomy using a custom-designed device based on a novel computer simulation system. *Journal of Orthopaedic Science*, 16(1):85–92, January 2011.
5. Biao Li, Lei Zhang, Hao Sun, Jianbing Yuan, Steve G.F. Shen, and Xudong Wang. A novel method of computer aided orthognathic surgery using individual CAD/CAM templates: a combination of osteotomy and repositioning guides. *British Journal of Oral and Maxillofacial Surgery*, 51(8):e239–e244, December 2013.
6. Lorenzo Guariento, Francesco Buonamici, Antonio Marzola, Rocco Furferi, and Yary Volpe. A Semi-Automatic CAD Procedure to Design Custom-made Surgical Cutting Guides. *Computer-Aided Design and Applications*, 19:733–740, November 2021.
7. L. Ulrich, F. Baldassarre, F. Marcolin, S. Moos, S. Tornincasa, E. Vezzetti, D. Speranza, G. Ramieri, and E. Zavattero. A Procedure for Cutting Guides Design in Maxillofacial Surgery: A Case-Study. In Francisco Cavas-Martínez, Benoit Eynard, Francisco J. Fernández Cañavate, Daniel G. Fernández-Pacheco, Paz Morer,

and Vincenzo Nigrelli, editors, *Advances on Mechanics, Design Engineering and Manufacturing II*, Lecture Notes in Mechanical Engineering, pages 301–310, Cham, 2019. Springer International Publishing.

8. Maryam Tilton, Gregory S. Lewis, Hwa Bok Wee, April Armstrong, Michael W. Hast, and Guha Manogharan. Additive manufacturing of fracture fixation implants: Design, material characterization, biomechanical modeling and experimentation. *Additive Manufacturing*, 33:101137, May 2020.
9. Silvia Izabella Pop, Mircea Dudescu, Sorin Gheorghe Mihali, Mariana Păcurar, and Dana Cristina Bratu. Effects of Disinfection and Steam Sterilization on the Mechanical Properties of 3D SLA- and DLP-Printed Surgical Guides for Orthodontic Implant Placement. *Polymers*, 14(10):2107, January 2022. Number: 10 Publisher: Multidisciplinary Digital Publishing Institute.
10. Subhrajit Ray, Arun Rout, and Ashok Sahoo. A comparative analysis of the abrasion wear characteristics of industrial wastes filled glass/polyester composites based on the design of experiment and neural network. *Polymer Composites*, 42(1):424–438, January 2021.
11. Lambert J. Stumpel. Deformation of Stereolithographically Produced Surgical Guides: An Observational Case Series Report: Deformation of Stereolithographically Produced Surgical Guides. *Clinical Implant Dentistry and Related Research*, 14(3):442–453, June 2012.
12. Hesham F. Marei, Alaa Alshaia, Sundus Alarifi, Naif Almasoud, and Adel Abdelhady. Effect of Steam Heat Sterilization on the Accuracy of 3D Printed Surgical Guides. *Implant Dentistry*, 28(4):372–377, August 2019.
13. Farusil Najeeb Mullaveettil, Rolanas Dauksevicius, and Yosef Wakjira. Strength and elastic properties of 3D printed PVDF-based parts for lightweight biomedical applications. *Journal of the Mechanical Behavior of Biomedical Materials*, 120:104603, August 2021.
14. M Robiony, F Polini, F Costa, T Vercellotti, and M Politi. Piezoelectric bone cutting in multipiece maxillary osteotomies. *Journal of Oral and Maxillofacial Surgery*, 62(6):759–761, June 2004.
15. Vladimir Pejaković, Robin Jisa, and Friedrich Franek. *Abrasion resistance of selected commercially available polymer materials*. Journal.fi, June 2014.
16. M. Á Aloy, J. E. Adsuara, P. Cerdá-Durán, M. Obergaulinger, J. J. Esteve-Taboada, T. Ferrer-Blasco, and R. Montés-Micó. Estimation of the mechanical properties of the eye through the study of its vibrational modes. *PLOS ONE*, 12(9):e0183892, September 2017. Publisher: Public Library of Science.
17. Krzysztof Zerdzicki, Pawel Lemski, Pawel Klosowski, Andrzej Skorek, Marcin Zmuda Trzebiatowski, and Mateusz Koberda. Tensile modulus of human orbital wall bones cut in sagittal and coronal planes. *PLOS ONE*, 16(11):e0259363, November 2021. Publisher: Public Library of Science.
18. Aisling Ni Annaidh, Karine Bruyere, Michel Destrade, Michael D. Gilchrist, and Melanie Ottenio. Characterising the Anisotropic Mechanical Properties of Excised Human Skin. *Journal of the Mechanical Behavior of Biomedical Materials*, 5(1):139–148, January 2012. arXiv:1302.3022 [cond-mat, physics:physics, q-bio].